ACS APPLIED MATERIALS & INTERFACES

www.acsami.org

Research Article

Synthesis of a Porous C_3N-Derived Framework with High Yield by Gallic Acid Cross-Linking Using Salt Melts

Zhihong Tian,* Tobias Heil, Johannes Schmidt, Shaokui Cao, and Markus Antonietti*

Cite This: *ACS Appl. Mater. Interfaces* 2020, 12, 13127−13133

Read Online

ACCESS | Metrics & More | Article Recommendations | Supporting Information

ABSTRACT: Porous carbon/nitrogen frameworks are an emerging class of noble organic materials with a wide range of potential applications. However, the design and controlled synthesis of those materials are still a challenge. Herein, we present the rational design of such a system with high microporosity, specific surface areas of up to 946 m^2 g^{-1}, and excellent condensation yields. The obtained noble frameworks were used for the delivery of larger organic molecules and changed the melting behavior of some daily drug molecules along their highly polarizable surfaces.

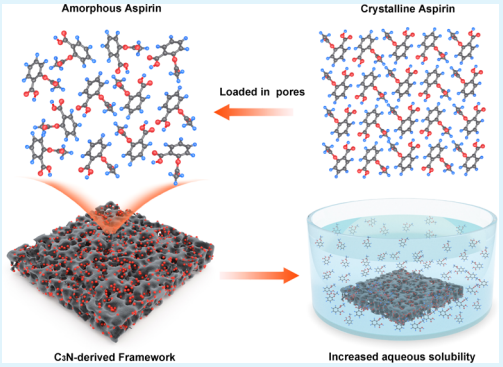

KEYWORDS: *C_3N-GA framework, functional pores, salt melt method, nanomedicine, solubility*

INTRODUCTION

In recent work, our group showed that carbonaceous materials[1] by appropriate heteroatom doping can show very positive highest occupied molecular orbital positions. The materials thereby behave "noble", i.e., are oxidation-stable under most conditions. Such noble, heteroatom-doped carbons not only inspire new science but also motivate many possible applications such as (metal-free) catalysis and noninnocent catalytic supports,[2,3] electrocatalysts for the oxygen reduction reaction,[4,5] battery electrodes,[6] or their use in high-voltage supercapacitors.[7] Noble carbons can be made from appropriate, also oxidation-stable, educts by thermodynamic "locking" of the band position, and even the local connectivity patterns are selected and optimized by this energy-directed synthesis.

The regular introduction of nitrogen into the carbon framework is also a reasonable method for the formation of carbon nitrides with different stoichiometries.[8] Graphitic C_3N_4, a crystalline material widely studied since 2009, can be peeled off to form a graphene-like porous sheet with abundant N atoms.[9,10] Recently, another ordered carbon nitride material, C_2N-*h*2D, was reported.[11] Similar to graphitic C_3N_4, C_2N-*h*2D consists of a regular arrangement of N6 cavities due to its high N content. The 2D crystalline structure and semiconductivity (with a direct band gap of 1.96 eV) of C_2N-*h*2D make it possible to become a better semiconductor than C_3N_4.[10] A 2D crystalline C_3N material was also synthesized by the thermolysis of *m*-phenylenediamine[12] and polymerization of 2,3-diaminophenazine[13] or by the pyrolysis of hexaaminobenzene trihydrochloride single crystals.[14] This material has a number of exciting properties, one among them is organic magnetism; it is not porous but is dense in covalent 2d-planes. It is to be assumed that these three C_xN_y species are just the beginning of a much bigger family of related compounds.

Recently, our group has synthesized a series of regular carbon materials close to the C_2N configuration with a specific pore structure and chemical composition by selecting suitable sustainable monomers and simple reaction methods.[15] In spite of the simplicity and scalability of the synthesis, some properties were found to be outstanding, such as the CO_2 adsorption capability and CO_2/N_2 adsorption selectivity. This was accredited to their surface chemistry and well-defined porosity.[16,17] The present work is based on the rules identified in this paper and will try to make a porous C_3N framework by using gallic acid as a co-monomer for branching, as it will be shown with a regular pore structure and a high heteroatom content. Potential applications instrumentalizing the slightly larger pore size will be presented here for the property change of organic compounds in such pores.

C_3N has a very nice but hole-free 2D crystalline structure composed of three phenyl rings sharing six N atoms. Due to the missing porosity and the low specific surface area, its

Received: November 11, 2019
Accepted: February 24, 2020
Published: February 24, 2020

https://dx.doi.org/10.1021/acsami.9b20478
ACS Appl. Mater. Interfaces 2020, 12, 13127−13133

Scheme 1. Idealized Structure of the C_3N-GA Framework

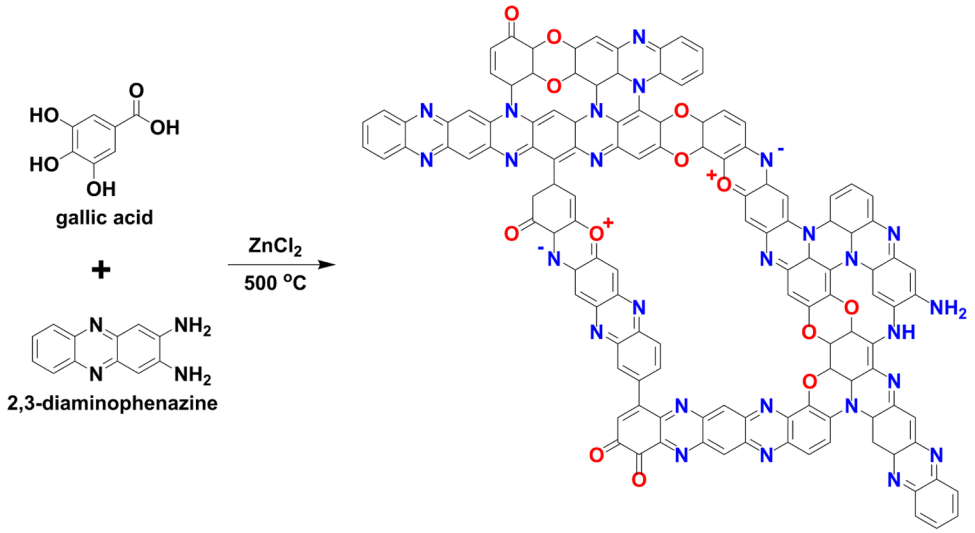

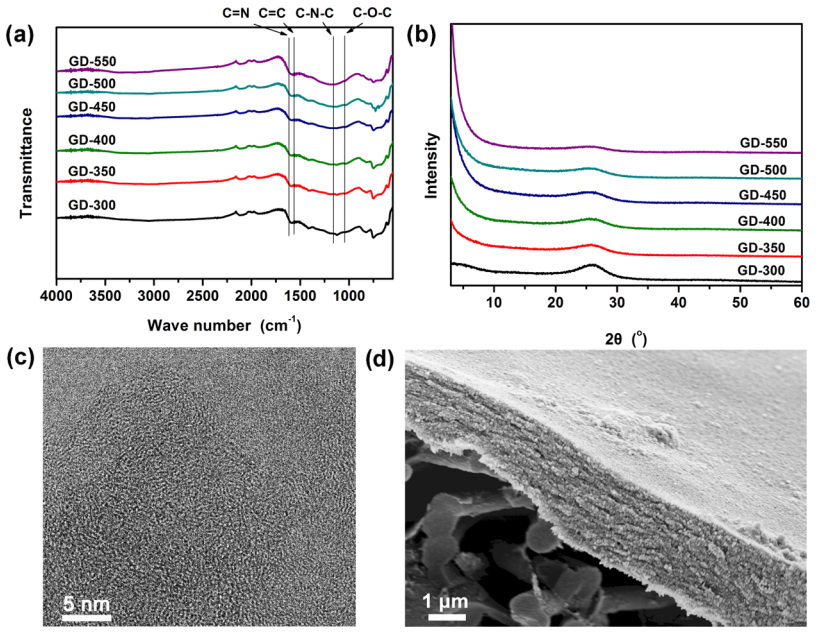

Figure 1. (a) FTIR spectra and (b) XRD of the GD-300, 350, 400, 450, 500, and 550 °C. (c) HRTEM image of GD-500. (d) SEM image of GD-500 on carbon fibers.

application in adsorption, catalysis, energy storage, etc. is limited. This is why we want to transport some of the C_3N-properties to a porous framework with gallic acid-based nodes. Scheme 1 depicts the explored approach: 2,3-diaminophenazine, the monomer known to polymerize into C_3N in the highest yield, forms typical connector structures, while gallic acid is then expected to add structural holes and oxygen moieties into the co-framework, very similar to the reactions described in ref 15. For that, a series of C_3N-GA framework materials are synthesized in salt melts using equimolar amounts of gallic acid and 2,3-diaminophenazine at different condensation temperatures varying from 300 to 850 °C. The resulting condensation products are labeled GD-300 to GD-850. It will be shown that these GDs indeed exhibit high porosity and good affinity to guest molecules, which will be illustrated by the interaction with a series of simple drug molecules, thus proposing a new type of organic delivery.

RESULTS AND DISCUSSION

Characterization of Materials. In the process of synthesizing GDs, $ZnCl_2$ was chosen as both the catalyst and solvent for the condensation reaction. In the molten salt, the gallic acid decarboxylates to produce pyrogallol,[18] which then reacts with 2,3-diaminophenazine to generate the extended 3D interpenetrated covalent structure (Scheme 1). Typically, the syntheses are carried out by stirring gallic acid (0.85 g, 5 mmol) and 2,3-diaminophenazine (1.05 g, 5 mmol) in $ZnCl_2$ (19 g), followed by condensation for 3 h at the target temperature (300−850 °C) and under an N_2 atmosphere to give a black product/salt mixture. The salt is separated by simple washing with water and filtration. It should be noted that the condensation yield is unusually high for such reactions (subtracting CO_2, water, and ammonia molecules along with previously discussed mechanisms, the theoretical yield is 79%). The mass yield after the reaction at 550 °C is 73% and still

https://dx.doi.org/10.1021/acsami.9b20478
ACS Appl. Mater. Interfaces 2020, 12, 13127−13133

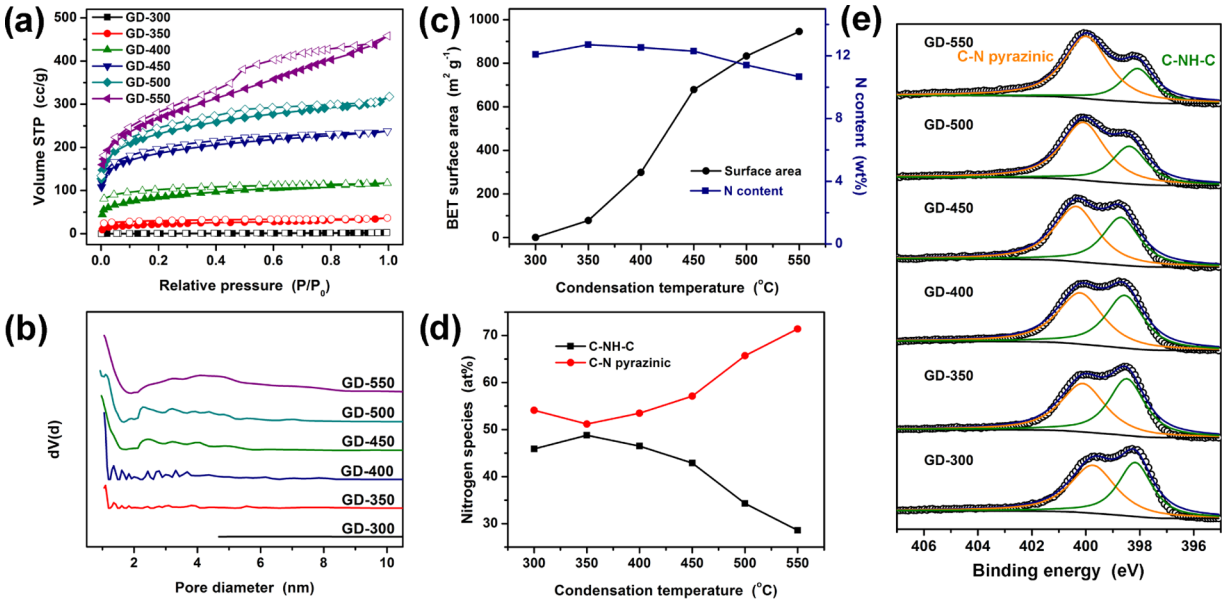

Figure 2. (a, b) N_2 adsorption and desorption isotherms at 77 K and pore size distribution curves calculated by QSDFT for GD-300, 350, 400, 450, 500, and 550. (c) Nitrogen content and S_{BET} of GD-300, 350, 400, 450, 500, and 550. (d, e) Nitrogen species compositions and the XPS N 1s spectra of GD-300, 350, 400, 450, 500, and 550.

64% even at a condensation temperature of 850 °C, i.e., practically no carbon fragments are lost throughout condensation. This high condensation yield indicates that gallic acid and 2,3-diaminophenazine indeed are perfect building blocks with defined thermal condensation chemistry to progress toward the desired C_3N-GA framework.

A variety of methods have been employed for the structural characterization of the new materials. Fourier transform infrared (FTIR) spectra of GDs exhibited peaks at around 1614, 1558, 1157, and 1043 cm^{-1}, which are characteristic of C═N, C═C, C−N−C, and C−O−C bonds,[19] thus confirming the occurrence of condensation (Figure 1a). The X-ray diffraction (XRD) patterns of all of the samples display only one broad diffraction peak at about 26°, indicating the absence of a long-range ordered structure (Figure 1b), which indeed is getting even weaker at higher condensation temperatures.[20] This excludes the presence of classical carbonization or graphitization and speaks for weakly packed, layered structures. This is also confirmed by high-resolution transmission electron microscopy (HRTEM), which observes sheetlike covalent materials without clear graphitic packing motifs, as shown for GD-500 (Figure 1c).

The morphological structures of GD-300 and GD-500 are investigated by scanning electron microscopy (SEM). GD-300 and GD-500 show essentially flat, crack-free material surfaces, in addition to some aggregates of primary nanoparticles (Figures 1d and S1). This is only possible with such a high carbonization yield. GD-500 is further characterized by various spectroscopies (Figure S2). A homogeneous distribution of C, N, and O in GD-500 is confirmed by the elemental mapping images. The high thermal stability shown by GDs is worth noting, as reflected in the thermogravimetric analysis (TGA) in the air (Figure S3). All of the samples even at a condensation temperature as low as 300 °C show a typical feature of nobility and have high oxidation and fragmentation resistance.[21] This can be ascribed to the homogeneous condensation scheme and the well-positioned presence of larger amounts of N and O heteroatoms.[15,22,23]

The permanent porosity of GDs is determined by N_2 adsorption−desorption isotherms at 77 K. As can be seen in Figure 2a, the BET surface area of samples increases from 0.7 (300 °C) to 946 $m^2\ g^{-1}$ (550 °C) with the increase of temperature. The adsorption isotherms of GD-450 and GD-500 show steep N_2 uptake at low relative pressure, thus indicating abundant micropore structures. Both of them have the highest relative microporosity of 67% (S_{mic}/S_{BET}) (Table S1). N_2 adsorption and desorption isotherms of GD-550 showed an obvious hysteresis loop in the steep region at P/P_0 = 0.45, indicating that interlamellar delamination is generated at 550 °C, in agreement with the XRD data. The Brunauer−Emmett−Teller (BET) surface area is 78 $m^2\ g^{-1}$ for GD-350, 299 $m^2\ g^{-1}$ for GD-400, 679 $m^2\ g^{-1}$ for GD-450, and 833 $m^2\ g^{-1}$ for GD-500 (Table S1). The S_{mic} value increases going from GD-350 (35 $m^2\ g^{-1}$) to GD-500 (562 $m^2\ g^{-1}$) and starts to decrease at 550 °C (522 $m^2\ g^{-1}$), which reveals that the well-defined micropores start to form at 350 °C and their formation is completed at 500 °C. As compared to our previous materials or other covalent frameworks, the specific surface area is slightly lower, thus underlining the thicker C_3N-like wall structure, as indicated in Scheme 1. Diaminophenazine at least dimerizes for framework formation, thus giving the essential chemical features for this structure.

The pore-size distributions of GDs are calculated by the quenched solid density functional theory (QSDFT) method (Figures 2b and S4), and they show hierarchical pores with interconnected or stacked narrow, structural micropores (1 nm) and a second, broader pore size distribution of 2−8 nm, which we attribute to delamination, as already observed in the thermal treatment of CTFs.[24] From Figure S5, it can be observed that higher condensation temperatures (850 °C) give rise to higher pore volumes and increased pore sizes due to a slight structural decomposition (10 wt % further mass), which we attribute to further delamination. However, because of the high stability of the skeleton, the N_2 adsorption−desorption isotherms and pore-size distribution curves maintain a similar

https://dx.doi.org/10.1021/acsami.9b20478
ACS Appl. Mater. Interfaces 2020, 12, 13127−13133

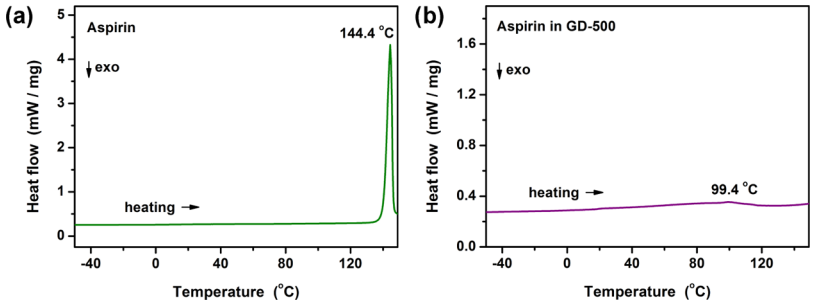

Figure 3. DSC records of the samples: (a) aspirin and (b) aspirin with GD-500.

shape compared to the 550 °C sample, and the specific surface area remains high at 921 m^2 g^{-1}.

Since the measurement of low-pressure nitrogen physisorption in such polar materials can be affected by the high quadrupole moment of nitrogen and thus leads to larger errors in determining the size of the micropores, we performed argon physisorption at 87 K to exemplarily determine the micropore size of the sample GD-500 (Figure S6). The shape of the isotherm is comparable to the nitrogen measurements, and the average micropore size of GD-500 was determined to be 1.3 nm.

We make the assumption that if 1 mol of gallic acid is reacting with 1 mol of 2,3-diaminophenazine, the expected composition of the product will be $C_{18}N_3O_2$ (the decarboxylation is calculated out), and the N contents in the framework will be 13.9 wt %. From the elemental analysis (Table S2), the N contents (indeed around 12 wt %) of GDs are not too far from the expected theoretical values, which means only a small amount of N is lost due to ammonia elimination during the process of condensation at high temperature. Because of the rather pure reaction, the structure of GDs is very close to the drawn framework structure as shown in Scheme 1. Therefore, micropores have been indeed successfully introduced into the C_3N structure through a one-to-one reaction between gallic acid and 2,3-diaminophenazine. The contents of N in GD-300, GD-350, GD-400, GD-450, GD-500, and GD-550 are analyzed to be 12.09, 12.71, 12.53, 12.30, 11.41, and 10.67 wt %, respectively (Table S2). These results indicate that the binary structure of the framework is very temperature-stable and hardly contains functional side groups that are easy to eliminate, as there is no significant decay of the heteroatoms with an increase of the condensation temperature. This result is very consistent with the result of TGA. In contrast, the specific surface area of GDs increases sharply while maintaining a similar chemical composition (Figure 2c). Thus, the porosity of the materials does not come from the decomposition of the framework and structural defects but mainly comes from the formation of larger than accessible arrays of aromatics in the materials' skeleton by structural ripening.

To further examine the compositional feature, X-ray photoelectron spectroscopy is performed for GD-300 to GD-550. The high-resolution O 1s XPS spectra can be deconvoluted into three peaks at 533, 531.8, and 530.7 eV (Figure S7), corresponding to O^+, C−O−C, and C═O, respectively.[15] This indicates again the formation of aromatic systems with a (+)-charge at the O atoms. Figure 2e shows that the peaks at 399.8 and 398.4 eV can be assigned to nitrogen in aromatic rings and secondary amine groups in the para position of O/N, respectively.[11] Furthermore, the atomic ratios of the two nitrogen configurations of N in C−N pyrazinic motifs and secondary C−NH−C motifs obtained from XPS results are plotted as a function of the condensation temperature (Figure 2d). As the temperature increases, more nitrogen is converted into pyrazinic N motifs, which are relevant to create conjugated aromatic systems during the process of condensation.

These materials are as such promising as electrodes and also show favorable gas sorption behavior (data not reported here), but we want to report here on the unusual uptake and physical behavior of medium-sized organic molecules in such frameworks.

Drug Loading and Solid-State Characterization. It is a commonly known problem that many newly invented potential drug candidates have good biological activity; however, their poor aqueous solubility hinders their clinical application.[25,26] Increasing the water solubility can improve drug availability and reduce side effects, as well as potentially reduce the dose required to achieve the same therapeutic effect. Changing the drug polymorph or even crystallinity as such is one of the simplest strategies to overcome this obstacle with changing the drug molecule, as solubility is hindered by the crystallization enthalpy.[27] We choose aspirin, a known model compound without larger toxicity, which is a white crystalline powder. It is slightly soluble in water to relieve mild or moderate pain but also used for fever, flu, and prevention of the onset of cardiovascular and cerebrovascular diseases. Improving solubility is known to promote the immediate onset of pain relief. We will use aspirin as a model and disperse it in the pores of GD-500 to examine the interaction between the nanoscale pores of the framework and aspirin molecules.

To confirm the physical state of aspirin, DSC is conducted; the curves are presented in Figure 3. In the case of parental bulk aspirin, a single sharp endothermic melting peak is observed at 144.4 °C. For the 37.5 wt % aspirin-loaded sample (30 mg of aspirin in 50 mg of GD-500), only a very weak and broad endothermic peak is visible around 99 °C, i.e., the sample is either molecularly adsorbed, amorphous, or only in the smallest crystalline cluster state.[28−30] This can be ascribed to the binding of aspirin molecules on the highly polarizable C_3N-GA framework surface in the presence of N and O. Furthermore, the encapsulated aspirin molecules are then unable to form a crystalline state in the nanometer-sized pores, instead of remaining in amorphous or liquid forms, which come with increased water solubility.[25,27,31] A C_3N-derived framework without gallic acid (D-500) is provided as a reference sample to better demonstrate the characteristics of GD-500. The nitrogen content of D-500 is significantly higher than that of GD-500 (Table S2). However, due to the nonporous nature of C_3N, its specific surface area is only 3 m^2

https://dx.doi.org/10.1021/acsami.9b20478
ACS Appl. Mater. Interfaces 2020, 12, 13127−13133

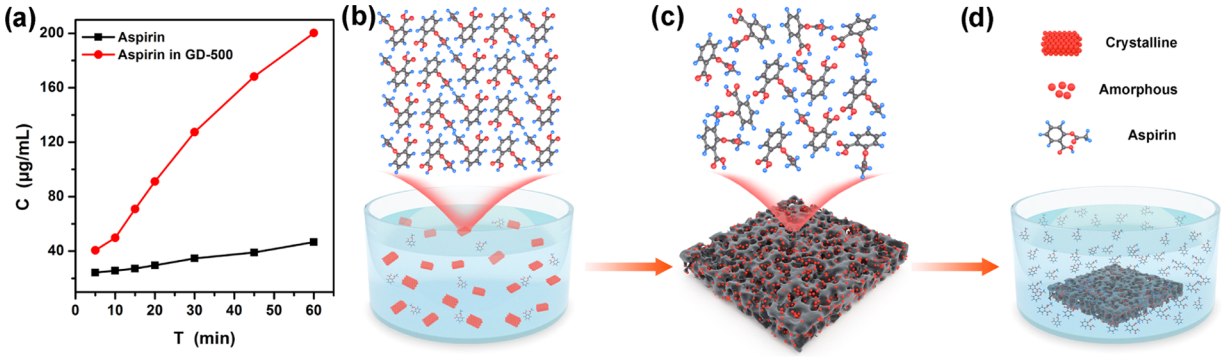

Figure 4. (a) Aspirin concentration−time profiles of the bulk aspirin and aspirin in GD-500. Schematic representation of (b) crystalline aspirin dissolution in water, (c) amorphous state after aspirin is loaded into the pores of GD-500, and (d) amorphous aspirin in GD-500 dissolution in water.

g^{-1} (Figure S8). As expected, a similar endothermic peak is also observed in the DSC curve of the aspirin with D-500 sample (Figure S9), indicating that the C_3N structure with a very small specific surface area does not modify or even influence the solid state of aspirin.[28] GD-500 has a high pore volume of 0.5 cm^3 g^{-1}, which contributes to high drug-loading contents. Indeed, elemental analysis results after loading aspirin drugs are very close to the theoretical values (Table S3). Obviously, highly polar micropores can be tightly filled with aspirin molecules, which then have a decreased or even no melting point.

DSC analysis of other medium-sized organic molecules loaded into GD-500 is used to further confirm the generality of this observation (Figures S10 and S11). As expected, all acetic-acid-, naphthalene-, and $HCOONH_4$-loaded GD-500 samples show significantly decreased melting peaks compared with bulk acetic acid, naphthalene, and $HCOONH_4$. In contrast, for Q10, an important cosmetic active well known from consumer applications, the melting peaks are practically unchanged in the Q10-loaded sample (Figure S12). Q10 is a big, rather unpolar molecule and is presumably prevented by size and polarity to enter the inner micropores of the GD skeleton. Similar behavior was observed for molten wax with a higher molecular weight and higher viscosity, and also here, the melting point showed almost no change after the wax was loaded onto the carrier (Figure S13). These results indicate that the pore structure and polarity are key factors that control the potential spatial distributions of organic molecules to bind and deliver, for instance, as drug carriers.[32,33]

The DSC results are also supported by XRD measurements (Figure S14). The XRD patterns of aspirin and aspirin with D-500 samples exhibit characteristic peaks corresponding to crystalline aspirin.[34] However, the characteristic crystalline peaks disappear in the XRD pattern of aspirin in GD-500, revealing that aspirin is completely present in an amorphous form.[35] This is attributed to the highly polarizable pore surface and finite-size effects, which provide enough interaction energy to prevent drug molecules entrapped in polar pore channels from rearranging themselves into a crystal lattice.[36] The FTIR spectra are recorded to detect the unloaded particles on the surface of GD-500 and D-500 (Figure S15). The spectra of aspirin with D-500 are similar to the bulk aspirin, which is caused by the aspirin adsorbed on the external surface or separate aspirin crystals. However, no significant peaks related to aspirin are found in the aspirin with GD-500 sample, which suggests that aspirin is loaded in the deeper pores of GD-500 and it lacked aggregated particles on the external surface.[37] These results are in good agreement with DSC and XRD data that the aspirin in the pores of GD-500 is completely in the amorphous state.

To further investigate the role of GD-500, a release profile of pure aspirin and aspirin-loaded GD-500 was recorded using purified water as dissolution medium. As shown in Figure 4a, the observed dissolution of pure aspirin is very limited in purified water (less than 47 μg/mL within 60 min). The slow dissolution is related to the crystalline form as confirmed by DSC and XRD studies and its very low solubility (Figure 4b). In the case of aspirin-loaded GD-500, a dramatic increase in the dissolution rate and extent (200 μg/mL within 60 min) is seen, especially when compared with that of pure aspirin. This outstanding increase in aspirin dissolution is clearly attributed to the improved dissolubility of amorphous aspirin present in the pores of GD-500 (Figure 4c,d). This phenomenon results from the factor that there is no lattice energy to be overcome.[38−40] Thus, such porous materials can be regarded as promising organic delivery materials.

CONCLUSIONS

We have reported the design and synthesis of a new series of porous copolymers made of gallic acid and 2,3-diaminophenazine building blocks connected through condensation reactions in salt melts. The reaction occurs with unprecedented mass yields, i.e., polycondensation occurs in a rather defined fashion, considering the extreme conditions involved. GD-500 shows a good BET surface area, high microporosity, and abundant N and O heteroatoms. Furthermore, strong polarization on carbon pore walls and well-defined pore structures in GD-500 lead to the incorporation of organic guest molecules, which cannot crystallize due to surface interactions and the quantum confinement effect. This is exemplified by effectively reducing the melting point of aspirin and three other small model compounds. The current work is related to the analysis of the redox properties and the electronic states of these materials.

ASSOCIATED CONTENT

Supporting Information

The Supporting Information is available free of charge at https://pubs.acs.org/doi/10.1021/acsami.9b20478.

Experimental section, SEM images (Figure S1), EDX mappings (Figure S2), thermal analysis of the samples (Figure S3), textural properties of the samples (Table

https://dx.doi.org/10.1021/acsami.9b20478
ACS Appl. Mater. Interfaces 2020, 12, 13127−13133

S1), cumulative QSDFT pore-size distribution curves (Figure S4), N_2 adsorption and desorption isotherms (Figures S5 and S8), Ar adsorption and desorption isotherms (Figure S6), elemental analysis of the samples (Tables S2 and S3), XPS O 1s spectra (Figure S7), DSC records (Figures S9−S13), XRD patterns (Figure S14), and FTIR spectra (Figure S15) (PDF)

AUTHOR INFORMATION

Corresponding Authors

Zhihong Tian − *School of Materials Science and Engineering, Zhengzhou University, Zhengzhou 450001, P. R. China; Department of Colloid Chemistry, Max Planck Institute of Colloids and Interfaces, Potsdam 14476, Germany;* orcid.org/0000-0002-6377-376X; Email: zhihong.tian@mpikg.mpg.de

Markus Antonietti − *Department of Colloid Chemistry, Max Planck Institute of Colloids and Interfaces, Potsdam 14476, Germany;* orcid.org/0000-0002-8395-7558; Email: office.cc@mpikg.mpg.de

Authors

Tobias Heil − *Department of Colloid Chemistry, Max Planck Institute of Colloids and Interfaces, Potsdam 14476, Germany*

Johannes Schmidt − *Technical University of Berlin, Institute of Chemistry, Berlin 10623, Germany*

Shaokui Cao − *School of Materials Science and Engineering, Zhengzhou University, Zhengzhou 450001, P. R. China*

Complete contact information is available at: https://pubs.acs.org/10.1021/acsami.9b20478

Author Contributions

The manuscript was written through contributions of all authors. All authors have given approval to the final version of the manuscript.

Notes

The authors declare no competing financial interest.

ACKNOWLEDGMENTS

The Max Planck Society is gratefully acknowledged for financial support. We thank Regina Rothe for technical assistance. Zhihong Tian sincerely acknowledges the financial support provided by Zhengzhou University and the National Natural Science Foundation of China (51873198).

REFERENCES

(1) Antonietti, M.; Oschatz, M. The Concept of "Noble, Heteroatom-Doped Carbons," Their Directed Synthesis by Electronic Band Control of Carbonization, and Applications in Catalysis and Energy Materials. *Adv. Mater.* **2018**, *30*, No. 1706836.

(2) Wang, Y.; Yao, J.; Li, H. R.; Su, D. S.; Antonietti, M. Highly Selective Hydrogenation of Phenol and Derivatives over a Pd@Carbon Nitride Catalyst in Aqueous Media. *J. Am. Chem. Soc.* **2011**, *133*, 2362−2365.

(3) Xue, Z. H.; Han, J. T.; Feng, W. J.; Yu, Q. Y.; Li, X. H.; Antonietti, M.; Chen, J. S. Tuning the Adsorption Energy of Methanol Molecules Along Ni-N-Doped Carbon Phase Boundaries by the Mott-Schottky Effect for Gas-Phase Methanol Dehydrogenation. *Angew. Chem., Int. Ed.* **2018**, *57*, 2697−2701.

(4) Shui, J. L.; Wang, M.; Du, F.; Dai, L. M. N-Doped Carbon Nanomaterials are Durable Catalysts for Oxygen Reduction Reaction in Acidic Fuel Cells. *Sci. Adv.* **2015**, *1*, No. e1400129.

(5) Liang, H. W.; Zhuang, X. D.; Bruller, S.; Feng, X. L.; Mullen, K. Hierarchically Porous Carbons with Optimized Nitrogen Doping as Highly Active Electrocatalysts for Oxygen Reduction. *Nat. Commun.* **2014**, *5*, No. 4973.

(6) Wang, L.; Yang, C. L.; Dou, S.; Wang, S. Y.; Zhang, J. T.; Gao, X.; Ma, J. M.; Yu, Y. Nitrogen-Doped Hierarchically Porous Carbon Networks: Synthesis and Applications in Lithium-Ion Battery, Sodium-Ion Battery and Zinc-Air Battery. *Electrochim. Acta* **2016**, *219*, 592−603.

(7) Salanne, M.; Rotenberg, B.; Naoi, K.; Kaneko, K.; Taberna, P. L.; Grey, C. P.; Dunn, B.; Simon, P. Efficient Storage Mechanisms for Building Better Supercapacitors. *Nat. Energy* **2016**, *1*, 16070.

(8) Sakaushi, K.; Antonietti, M. Carbon- and Nitrogen-Based Organic Frameworks. *Acc. Chem. Res.* **2015**, *48*, 1591−1600.

(9) Wang, X. C.; Maeda, K.; Thomas, A.; Takanabe, K.; Xin, G.; Carlsson, J. M.; Domen, K.; Antonietti, M. A Metal-Free Polymeric Photocatalyst for Hydrogen Production from Water under Visible Light. *Nat. Mater.* **2009**, *8*, 76−80.

(10) Liu, J.; Liu, Y.; Liu, N. Y.; Han, Y. Z.; Zhang, X.; Huang, H.; Lifshitz, Y.; Lee, S. T.; Zhong, J.; Kang, Z. H. Metal-Free Efficient Photocatalyst for Stable Visible Water Splitting via a Two-Electron Pathway. *Science* **2015**, *347*, 970−974.

(11) Mahmood, J.; Lee, E. K.; Jung, M.; Shin, D.; Jeon, I. Y.; Jung, S. M.; Choi, H. J.; Seo, J. M.; Bae, S. Y.; Sohn, S. D.; Park, N.; Oh, J. H.; Shin, H. J.; Baek, J. B. Nitrogenated Holey Two-Dimensional Structures. *Nat. Commun.* **2015**, *6*, No. 6486.

(12) King, T. C.; Matthews, P. D.; Holgado, J. P.; Jefferson, D. A.; Lambert, R. M.; Alavi, A.; Wright, D. S. A Single-Source Route to Bulk Samples of C_3N and The Co-Evolution of Graphitic Carbon Microspheres. *Carbon* **2013**, *64*, 6−10.

(13) Yang, S. W.; Li, W.; Ye, C. C.; Wang, G.; Tian, H.; Zhu, C.; He, P.; Ding, G. Q.; Xie, X. M.; Liu, Y.; Lifshitz, Y.; Lee, S. T.; Kang, Z. H.; Jiang, M. H. C_3N-A 2D Crystalline, Hole-Free, Tunable-Narrow-Bandgap Semiconductor with Ferromagnetic Properties. *Adv. Mater.* **2017**, *29*, No. 1605625.

(14) Mahmood, J.; Lee, E. K.; Jung, M.; Shin, D.; Choi, H. J.; Seo, J. M.; Jung, S. M.; Kim, D.; Li, F.; Lah, M. S.; Park, N.; Shin, H. J.; Oh, J. H.; Baek, J. B. Two-Dimensional Polyaniline (C_3N) from Carbonized Organic Single Crystals in Solid State. *Proc. Natl. Acad. Sci. USA* **2016**, *113*, 7414−7419.

(15) Tian, Z. H.; Fechler, N.; Oschatz, M.; Heil, T.; Schmidt, J.; Yuan, S. G.; Antonietti, M. $C_2N_xO_{1-X}$ Framework Carbons with Defined Microporosity and Co-Doped Functional Pores. *J. Mater. Chem. A* **2018**, *6*, 19013−19019.

(16) Das, P.; Mandal, S. K. In-Depth Experimental and Computational Investigations for Remarkable Gas/Vapor Sorption, Selectivity, and Affinity by a Porous Nitrogen-Rich Covalent Organic Framework. *Chem. Mater.* **2019**, *31*, 1584−1596.

(17) Jena, H. S.; Krishnaraj, C.; Wang, G.; Leus, K.; Schmidt, J.; Chaoui, N.; Van Der Voort, P. Acetylacetone Covalent Triazine Framework: An Efficient Carbon Capture and Storage Material and A Highly Stable Heterogeneous Catalyst. *Chem. Mater.* **2018**, *30*, 4102−4111.

(18) Xia, Z.; Singh, A.; Kiratitanavit, W.; Mosurkal, R.; Kumar, J.; Nagarajan, R. Unraveling The Mechanism of Thermal and Thermo-Oxidative Degradation of Tannic Acid. *Thermochim. Acta* **2015**, *605*, 77−85.

(19) Wang, L. P.; Wu, X. Q.; Guo, S. J.; Han, M. M.; Zhou, Y. J.; Sun, Y.; Huang, H.; Liu, Y.; Kang, Z. H. Mesoporous Nitrogen, Sulfur Co-Doped Carbon Dots/Cos Hybrid as an Efficient Electrocatalyst for Hydrogen Evolution. *J. Mater. Chem. A* **2017**, *5*, 2717−2723.

(20) Li, Y. J.; Zheng, S. H.; Liu, X.; Li, P.; Sun, L.; Yang, R. X.; Wang, S.; Wu, Z. S.; Bao, X. H.; Deng, W. Q. Conductive Microporous Covalent Triazine-Based Framework for High-Performance Electrochemical Capacitive Energy Storage. *Angew. Chem., Int. Ed.* **2018**, *57*, 7992−7996.

(21) Walczak, R.; Kurpil, B.; Savateev, A.; Heil, T.; Schmidt, J.; Qin, Q.; Antonietti, M.; Oschatz, M. Template- and Metal-Free Synthesis of Nitrogen-Rich Nanoporous "Noble" Carbon Materials by Direct Pyrolysis of a Preorganized Hexaazatriphenylene Precursor. *Angew. Chem., Int. Ed.* **2018**, *57*, 10765−10770.

(22) Zhang, S. G.; Tsuzuki, S.; Ueno, K.; Dokko, K.; Watanabe, M. Upper Limit of Nitrogen Content in Carbon Materials. *Angew. Chem., Int. Ed.* **2015**, *54*, 1302−1306.
(23) Paraknowitsch, J. P.; Thomas, A. Doping Carbons beyond Nitrogen: An Overview of Advanced Heteroatom Doped Carbons with Boron, Sulphur and Phosphorus for Energy Applications. *Energy Environ. Sci.* **2013**, *6*, 2839−2855.
(24) Kuhn, P.; Forget, A.; Su, D. S.; Thomas, A.; Antonietti, M. From Microporous Regular Frameworks to Mesoporous Materials with Ultrahigh Surface Area: Dynamic Reorganization of Porous Polymer Networks. *J. Am. Chem. Soc.* **2008**, *130*, 13333−13337.
(25) Vasconcelos, T.; Sarmento, B.; Costa, P. Solid Dispersions as Strategy to Improve Oral Bioavailability of Poor Water Soluble Drugs. *Drug Discovery Today* **2007**, *12*, 1068−1075.
(26) Chen, K.; Mitra, S. Incorporation of Functionalized Carbon Nanotubes into Hydrophobic Drug Crystals for Enhancing Aqueous Dissolution. *Colloids Surf., B* **2019**, *173*, 386−391.
(27) Brough, C.; Williams, R. O. Amorphous Solid Dispersions and Nano-Crystal Technologies for Poorly Water-Soluble Drug Delivery. *Int. J. Pharm.* **2013**, *453*, 157−166.
(28) Zhang, Y. Z.; Che, E. X.; Zhang, M.; Sun, B. X.; Gao, J.; Han, J.; Song, Y. L. Increasing the Dissolution Rate and Oral Bioavailability of the Poorly Water-Soluble Drug Valsartan using Novel Hierarchical Porous Carbon Monoliths. *Int. J. Pharm.* **2014**, *473*, 375−383.
(29) Liu, Y.; Wu, C.; Hao, Y. N.; Xu, J.; Zhao, Y.; Qiu, Y.; Jiang, J.; Yu, T.; Ji, P. Preparation of a Novel Starch-Derived Three-Dimensional Ordered Macroporous Carbon for Improving the Dissolution Rate and Oral Bioavailability of Water-Insoluble Drugs. *J. Pharm. Biomed. Anal.* **2016**, *118*, 267−275.
(30) Niu, X.; Wan, L.; Hou, Z.; Wang, T. Y.; Sun, C. S.; Sun, J.; Zhao, P.; Jiang, T. Y.; Wang, S. L. Mesoporous Carbon as a Novel Drug Carrier of Fenofibrate for Enhancement of the Dissolution and Oral Bioavailability. *Int. J. Pharm.* **2013**, *452*, 382−389.
(31) Zhang, Y.; Zhang, J. H.; Jiang, T. Y.; Wang, S. L. Inclusion of the Poorly Water-Soluble Drug Simvastatin in Mesocellular Foam Nanoparticles: Drug Loading and Release Properties. *Int. J. Pharm.* **2011**, *410*, 118−124.
(32) Zhang, G. Y.; Li, X. L.; Liao, Q. B.; Liu, Y. F.; Xi, K.; Huang, W. Y.; Jia, X. D. Water-Dispersible PEG-Curcumin/Amine-Functionalized Covalent Organic Framework Nanocomposites as Smart Carriers for in Vivo Drug Delivery. *Nat. Commun.* **2018**, *9*, No. 2785.
(33) Mitra, S.; Sasmal, H. S.; Kundu, T.; Kandambeth, S.; Math, K.; Diaz, D. D.; Banerjee, R. Targeted Drug Delivery in Covalent Organic Nanosheets (CONs) via Sequential Postsynthetic Modification. *J. Am. Chem. Soc.* **2017**, *139*, 4513−4520.
(34) Jain, H.; Khomane, K. S.; Bansal, A. K. Implication of Microstructure on the Mechanical Behaviour of an Aspirin−paracetamol Eutectic Mixture. *CrystEngComm* **2014**, *16*, 8471−8478.
(35) Sayed, E.; Karavasili, C.; Ruparelia, K.; Haj-Ahmad, R.; Charalambopoulou, G.; Steriotis, T.; Giasafaki, D.; Cox, P.; Singh, N.; Giassafaki, L. N.; Mpenekou, A.; Markopoulou, C. K.; Vizirianakis, I. S.; Chang, M.; Fatouros, D. G.; Ahmad, Z. Electrosprayed Mesoporous Particles for Improved Aqueous Solubility of a Poorly Water Soluble Anticancer Agent: in vitro and ex vivo Evaluation. *J. Controlled Release* **2018**, *278*, 142−155.
(36) Jackson, C. L.; McKenna, G. B. Vitrification and Crystallization of Organic Liquids Confined to Nanoscale Pores. *Chem. Mater.* **1996**, *8*, 2128−2137.
(37) Miriyala, N.; Ouyang, D.; Perrie, Y.; Lowry, D.; Kirby, D. J. Activated Carbon as a Carrier for Amorphous Drug Delivery: Effect of Drug Characteristics and Carrier Wettability. *Eur. J. Pharm. Biopharm.* **2017**, *115*, 197−205.
(38) Babu, N. J.; Nangia, A. Solubility Advantage of Amorphous Drugs and Pharmaceutical Cocrystals. *Cryst. Growth Des.* **2011**, *11*, 2662−2679.
(39) Yadavalli, T.; Ames, J.; Agelidis, A.; Suryawanshi, R.; Jaishankar, D.; Hopkins, J.; Thakkar, N.; Koujah, L.; Shukla, D. Drug-encapsulated Carbon (DECON): A Novel Platform for Enhanced Drug Delivery. *Sci. Adv.* **2019**, *5*, No. eaax0780.
(40) Wu, X.; Si, Y.; Zou, Y.; Mao, Y.; Li, Q.; Zhou, S.; Chen, M.; Wu, L. Dual-Porosity Hollow Carbon Spheres with Tunable Through-Holes for Multi-Guest Delivery. *ACS Appl. Mater. Interfaces* **2018**, *10*, 31664−31673.

https://dx.doi.org/10.1021/acsami.9b20478
ACS Appl. Mater. Interfaces 2020, 12, 13127−13133